ELSEVIER

Contents lists available at ScienceDirect

Mechanism and Machine Theory

journal homepage: www.elsevier.com/locate/mechmt





Design of an over-constraint based nearly-constant amplification ratio compliant mechanism[☆]

Jiaxiang Zhu^a, Guangbo Hao^{a,*}, Tinghao Liu^a, Haiyang Li^b

- ^a School of Engineering and Architecture, University College Cork, Cork T12 K8AF, Ireland
- ^b School of Automotive Engineering, Dalian University of Technology, No.2 Linggong Road, Ganjingzi District, Dalian 116024, China

ARTICLE INFO

Keywords: Compliant mechanisms Compliant amplifier Nonlinear analysis Constant amplification ratio Closed-form solution

ABSTRACT

A constant displacement amplification ratio is less investigated in compliant mechanisms. This study addresses this need by presenting an over-constraint based nearly-constant amplification ratio compliant mechanism (OCARCM) that alleviates the change in displacement amplification ratio. The free-body diagram (FBD) combined with the generic beam constraint model (BCM) method is employed to obtain the closed-form solutions that accurately and insightfully elaborate the nonlinear kinetostatic characteristics of the OCARCM. Comparative analysis is provided between the proposed OCARCM and the widely-used bridge-type compliant amplifier in terms of the ability to remain a constant amplification ratio, with and without external payloads. The closed-form models are verified by the nonlinear finite element results (FEA) with a maximum difference of 1%. In our case studies, it shows that the amplification ratio of the OCARCM changes by 1% over the range, while that of the bridge-type amplifier changes by approximately 14% under the same conditions. The results also reveal that a higher amplification ratio results in a greater variation in the ratio. An experiment based on the CNC machined aluminium alloy prototype with distributed-compliance is conducted, and experimental results show a maximum error of 3.4% for the amplification ratio compared with the analytical or FEA results.

1. Introduction

A compliant mechanism-based amplifier (compliant amplifier in short) can be used either as a motion amplification mechanism to increase the stroke of a device or as a motion reducer to increase the motion resolution. For example, the compliant-mechanism-based piezoelectric actuator incorporates a compliant stroke amplification mechanism to amplify the motion range since a piezoelectric actuator without an amplification mechanism can produce a stroke generally less than 0.1% of its length. Instead, the compliant amplifier can be incorporated into the piezoelectric actuator to achieve nano or even sub-nano resolution by swapping the input and output to achieve a resolution refinement. A compliant amplifier exhibits several merits due to being a compliant mechanism, such as wear-free, zero noise, zero backlash, and vacuum compatibility [1,2], which is essential in extensive applications, such as jet dispensing [3–5], energy harvesting [6–9], nanopositioner actuation [10–14]. Currently, three types of compliant amplifiers are being widely used, i.e., the bridge-type [4,10,15–19], the lever type [20–22], and their derivatives [8,12,23–26]. The bridge-type amplifier is

E-mail address: G.Hao@ucc.ie (G. Hao).

^{*} The original version of this paper has been presented at the ASME 2022 International Design Engineering Technical Conferences & Computers and Information in Engineering Conference IDETC—CIE 2022, with a paper number DETC2022-89,555. Copyright has been granted by ASME.

^{*} Corresponding author.

mostly used due to its compact and symmetric structure [27–29]. A quarter of the bridge-type compliant amplifier can be kinematically treated as a rigid-body double-slider mechanism (Fig. 1), whose instantaneous amplification ratio at the current configuration can be expressed as $1/\tan\varphi$ [30]. As the input displacement in the X-direction increases, the geometry parameter φ of the bridge-type compliant amplifier will change, which leads to the change of the amplification ratio. In particular, the amplification ratio of such a mechanism exhibits a sudden increase and a gradual decrease over the range of the input displacement [31]. The change of the amplification ratio in the bridge-type amplifier remains an open issue. However, it is important to understand the potential benefits of a constant amplification ratio in a compliant amplifier before considering alleviating the changes.

The concept of a constant amplification ratio in compliant amplifiers has received limited attention in previous research, with only a few papers mentioning it. In [18], the author states that a constant amplification ratio is desirable for motion reduction in order to achieve fine position adjustments. Additionally, in [32], the authors highlight the control consideration into the variable amplification ratio for achieving high-accuracy positioning. Although the applications of a constant amplification ratio have not been extensively studied, incorporating this feature into a compliant amplifier design can provide valuable insight into predicting the output motion. A tangible application would be desired in the generation of uniform output motion resolution/precision, over the whole range of motion, in micro-/nano-positioning. In such an application, the input motion resolution is usually constant and determined by the actuator (such as PZT), then the output motion resolution is also constant if the amplification ratio is also constant, leading to uniform output motion resolution/precision over the whole range of motion.

The theoretical model of a compliant amplifier has been previously investigated using various methods including the geometric model, linear model, and nonlinear model [33]. The geometric model simplifies compliant mechanisms as rigid links joined by the ideal pivots, where the amplification ratio is determined primarily by the slope of the link [30,34,35]. This leads to poor prediction accuracy due to excessive simplification. The linear model is the most popular modeling method since it balances the complexity and accuracy of the solutions [35–38]. However, it neglects the nonlinearities in force-displacement characteristics and largely compromises accuracy under large deformation. In this paper, the nonlinear modelling method based on the beam constraint model (BCM) will be used to offer a more accurate analysis of the characteristics of the compliant amplifier under large deflection. The BCM captures the elastic, load-stiffening, kinematic, and elastokinematic effects in compliant beams [39]. It can provide a comprehensive nonlinear analysis of the compliant amplifier, not only limited to an accurate amplification ratio prediction.

This work presents several main contributions:

- The constant amplification ratio is first studied in the design of a compliant amplifier.
- A novel over-constraint based nearly-constant amplification ratio compliant mechanism (OCARCM) is proposed, which is able to provide a nearly constant amplification ratio.
- The nonlinear closed-form solutions of the OCARCM are derived with the consideration of the effect of payloads.
- An experiment is conducted with the consideration of payload (using a loading spring) to mimic the actuation of a compliant mechanism.

The rest of this paper is organized as follows. Section 2 presents the design of the OCARCM based on the over-constraint method. Section 3 explores the nonlinear analytical modeling of the OCARCM underlying the BCM approach. The characteristics analysis with the verification of FEA results is presented in Section 4. The experiment based on a CNC machined prototype is conducted in Section 5. Finally, the conclusions are drawn in Section 5.

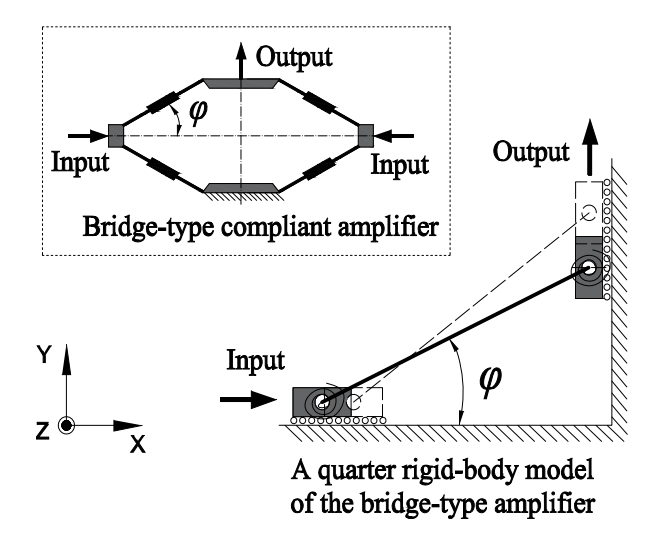


Fig. 1. A quarter of the bridge-type compliant amplifier with a nonconstant amplification ratio.

Fig. 2. Design from traditional rigid mechanism to compliant mechanism: (a) two rotationally symmetric double slider mechanism; (b) its compliant equivalent; (c) the over-constraint compliant mechanism.

 3

2. Mechanism design based on the over-constraint approach

In the literature, several compliant mechanism design approaches are available for the design of compliant amplifiers. For instance, researchers commonly use a multistage design method to achieve a large displacement or force amplification ratio [40–42]. Flexure hinges are preferred over distributed-compliance beams [43–45] in order to improve the dynamic performance or load capacity of the compliant amplifier. Distributed-compliance beams are commonly used to reduce stress concentration in the compliant amplifier. A symmetrical arrangement is a commonly used method to avoid parasitic motion [46–48]. The use of serial or parallel connection of flexure modules in a compliant amplifier can lead to possible improvement of performance characteristics such as amplification ratio, parasitic motion, and load capacity [40,49,22,43]. The over-constraint approach [50,51] usually involves adding extra constraints to the compliant mechanism, such as additional beams or links, to restrict its undesired motion or performance characteristics. In this section, we employ a new over-constraint method to eliminate the amplification ratio change of a compliant amplifier maximally.

The amplification ratio of the bridge-type compliant amplifier changes with the input displacement. As shown in Fig. 2(a), the α and β are the initial angles of the flexure beams. As the double slider mechanism at the bottom is actuated in the X-direction (the slope of the link alters from α to α '), the amplification ratio increases. The double slider on the top is the 180-degree rotated version of the one at the bottom. When it is being actuated in the same direction as the one at the bottom, the amplification ratio decreases since the slope of the beam increases from angle β to angle β '. So, the amplification ratio of the double slider on the top is decreasing while the bottom one is increasing. If we want to constrain the amplification ratio from altering, we can simply connect the input cranks and output cranks of both double slider mechanisms, leading to an over-constraint configuration. However, the over-constrained rigid mechanism does not have any degrees of freedom, so the next step is the flexure module embodiment. Fig. 2(b) shows the compliant designs of the two double slider mechanisms with parallel-arranged beams. By connecting their inputs/outputs with a rigid link, we can obtain the over-constraint compliant mechanism as shown in Fig. 2(c). The mechanism in Fig. 2(c) is a quarter of the bridge-type amplifier. The fully embodied amplifier, called OCARCM, is depicted in Fig. 3(a). The OCARCM is mainly composed of two input stages, output stages, a base, and eight generic flexure beams. The OCARCM is a highly effective solution that not only mitigates changes in the amplification ratio but also significantly enhances the in-plane rotational stiffness of both the input and output stages compared with the bridge-type amplifier. This better-restricted rotation attributes to the formed parallelograms in the over-constraint design, which provide additional stability to the system.

The geometric parameters of the OCARCM are labeled in Fig. 3(b), and we can notice that the geometry of the OCARCM is symmetric about the centerlines. The input force F_{IN} is assigned in the X-direction and the payload in the Y-direction is defined as F_{L} . It is also worth noting that only the compliant segments of the flexure beam are deformable, and the rest are rigid.

3. Nonlinear analytical modeling

3.1. Generalized flexure beam

Linear analytical modeling fails to capture nonlinear stiffness characteristics and can only be applied over a relatively small range of motion. In this section, the BCM [52] was used for a generalized beam flexure, serving to accurately model the characteristics of the proposed amplifier when combing with the free-body-diagram (FBD) system modelling method. The BCM approach captures nonlinearities and leads to a closed-form model that can accurately estimate the kinetostatic behavior of a generalized beam subjected to combined loads. It is necessary to solve equations associated with constitutive relationships, load-equilibrium conditions, and

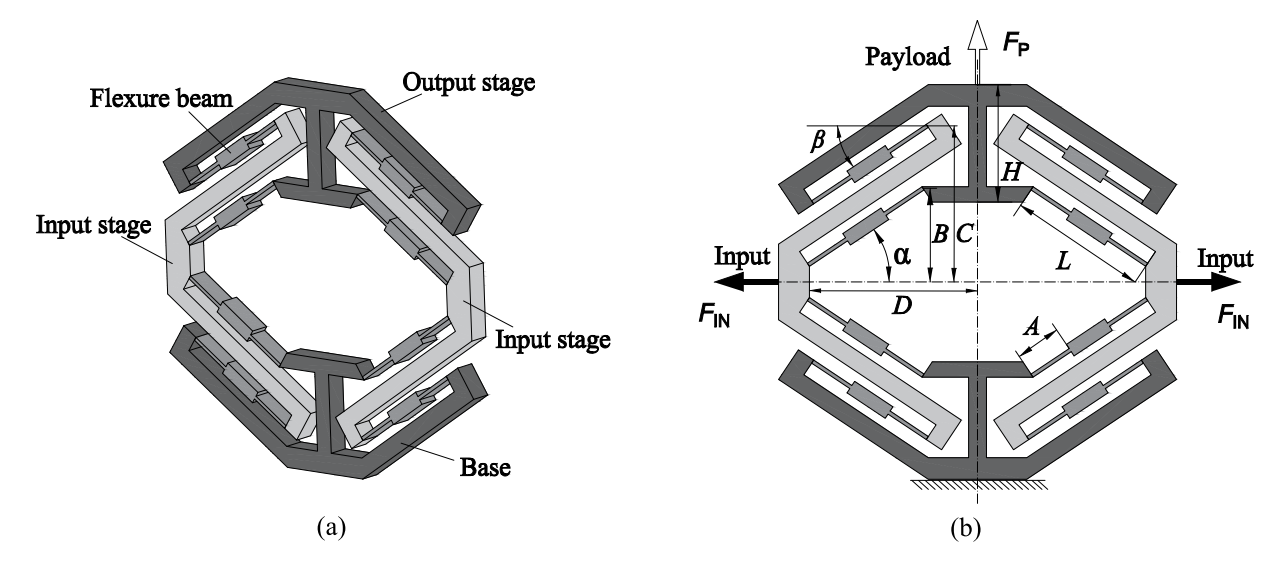


Fig. 3. A schematic of OCARCM design with parameter labelling: (a) isometric view; (b) the front view.

geometric compatibility conditions to obtain the load and displacement relationships of the proposed amplifier.

The generic flexure beams embodied in the amplifier are identical, one of which, in its deformed configuration, is shown in Fig. 4. The loading conditions for a single flexure beam are represented by F_i (axial force), P_i (transverse force), and M_i (moment) acting at the tip of the beam. The resulting displacements are represented by X_i (displacement along X-axis), Y_i (displacement along Y-axis), θ_i and (rotational angle along Z-axis) with the respect to the local coordinate frame. To simplify the equation representation, all length parameters and translational displacements are normalized by beam length L, forces by EI/L^2 , and moments by EI/L. Each of the normalized quantities is indicated in lowercase, specifically:

$$f_i = \frac{F_i}{EI/L^2}, p_i = \frac{P_i}{EI/L^2}, m_i = \frac{M_i}{EI/L}, x_i = \frac{X_i}{L}, y_i = \frac{Y_i}{L}, u = \frac{U}{L}, t = \frac{T}{L}$$
 (1)

where *I* is the second moment of area of the generic flexure beam cross-section about the Z-axis, and *E* denotes Young's modulus of the material. The constitutive equations of each flexure beam are represented below [53]:

$$\begin{bmatrix} f_i \\ m_i \end{bmatrix} = \begin{bmatrix} k_{11}^{(0)} & k_{12}^{(0)} \\ k_{21}^{(0)} & k_{22}^{(0)} \end{bmatrix} \begin{bmatrix} y_i \\ \theta_i \end{bmatrix} + p_i \begin{bmatrix} k_{11}^{(1)} & k_{12}^{(1)} \\ k_{21}^{(1)} & k_{22}^{(1)} \end{bmatrix} \begin{bmatrix} y_i \\ \theta_i \end{bmatrix}$$
(2)

$$x_{i} = \frac{p_{i}}{k_{33}} + \begin{bmatrix} y_{i} & \theta_{i} \end{bmatrix} \begin{bmatrix} g_{11}^{(0)} & g_{12}^{(0)} \\ g_{13}^{(0)} & g_{14}^{(0)} \end{bmatrix} \begin{bmatrix} y_{i} \\ \theta_{i} \end{bmatrix} + p_{i} \begin{bmatrix} y_{i} & \theta_{i} \end{bmatrix} \begin{bmatrix} g_{11}^{(1)} & g_{12}^{(1)} \\ g_{13}^{(1)} & g_{14}^{(1)} \end{bmatrix} \begin{bmatrix} y_{i} \\ \theta_{i} \end{bmatrix}$$

$$(3)$$

where the coefficients k and g are non-dimensional values that characterize the stiffness of a double-notch flexure beam, and they have been provided in [53]. It is also worth noting that coefficients/entries associated with the symbols, k and g, are the functions of g (Fig. 4). In the case of g = 1/2, the generic beam corresponds to a distributed-compliance beam, which will be further discussed in Section 4.

3.2. Kinetostatic analysis of the amplifier

As the OCARCM is geometrically symmetrical, a quarter of the geometry is used to synthesize its kinetostatic characteristics. The FBD of a quarter of the OCARCM is presented in Fig. 5(b), where the deformation is assumed to occur only in the flexure segments of the lumped-compliance beam, and the other parts are rigid. $f_{\rm in}$ and $f_{\rm p}$ labeled in Fig. 5 are the normalised input force and the payload, respectively. $m_{\rm x}$ and $m_{\rm y}$ are the supplementary moments to maintain the zero rotation of the input stage and output stage, respectively. Based on the constrained relations and the symmetric structure, the rotational displacement θ_i of the rigid stages in the amplifier is equal to zero. Then the constitutive equations can be simplified as:

$$\begin{cases} f_{i} = k_{11}^{(0)} y_{i} + p_{i} k_{11}^{(1)} y_{i} \\ x_{i} = \frac{p_{i}}{k_{33}} + g_{11}^{(0)} k_{11}^{(1)} y_{i}^{2} + p_{i} y_{i}^{2} g_{11}^{(1)} \\ m_{i} = p_{i} k_{21}^{(1)} y_{i} + k_{21}^{(0)} y_{i} \end{cases}$$

$$(4)$$

Given that the coefficient $k_{11}^{(1)}$ is equal to $-2g_{11}^{(0)}$, and $g_{11}^{(0)}$ is 400 orders of magnitude larger than $g_{11}^{(1)}$. The constitutive equation in the X-direction (Eq. (4)) can be further simplified by removing the third term for the practical interest of this paper.

The load-equilibrium conditions of each rigid stage can be derived from the free-body diagrams of the rigid stages shown in Fig. 5 (b). It is worth noting that the moment reference center is the geometry center *O* as labeled in Fig. 5(a).

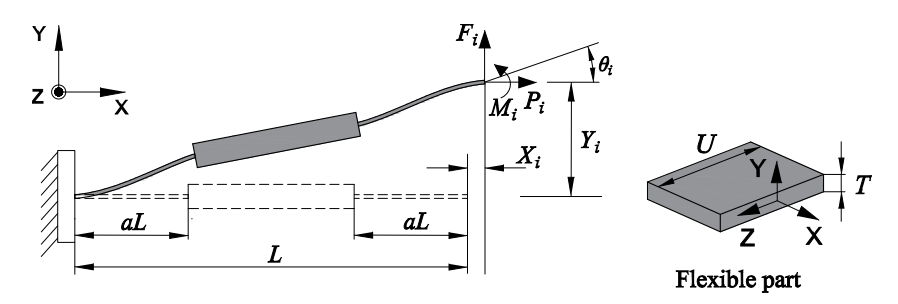


Fig. 4. Loading condition and geometry parameters of the generic flexure beam (the middle part considered to be rigid, with a thickness much larger than T); Under the condition of a = 1/2, the generic beam corresponds to a uniform thickness beam, i.e., distributed-compliance beam.

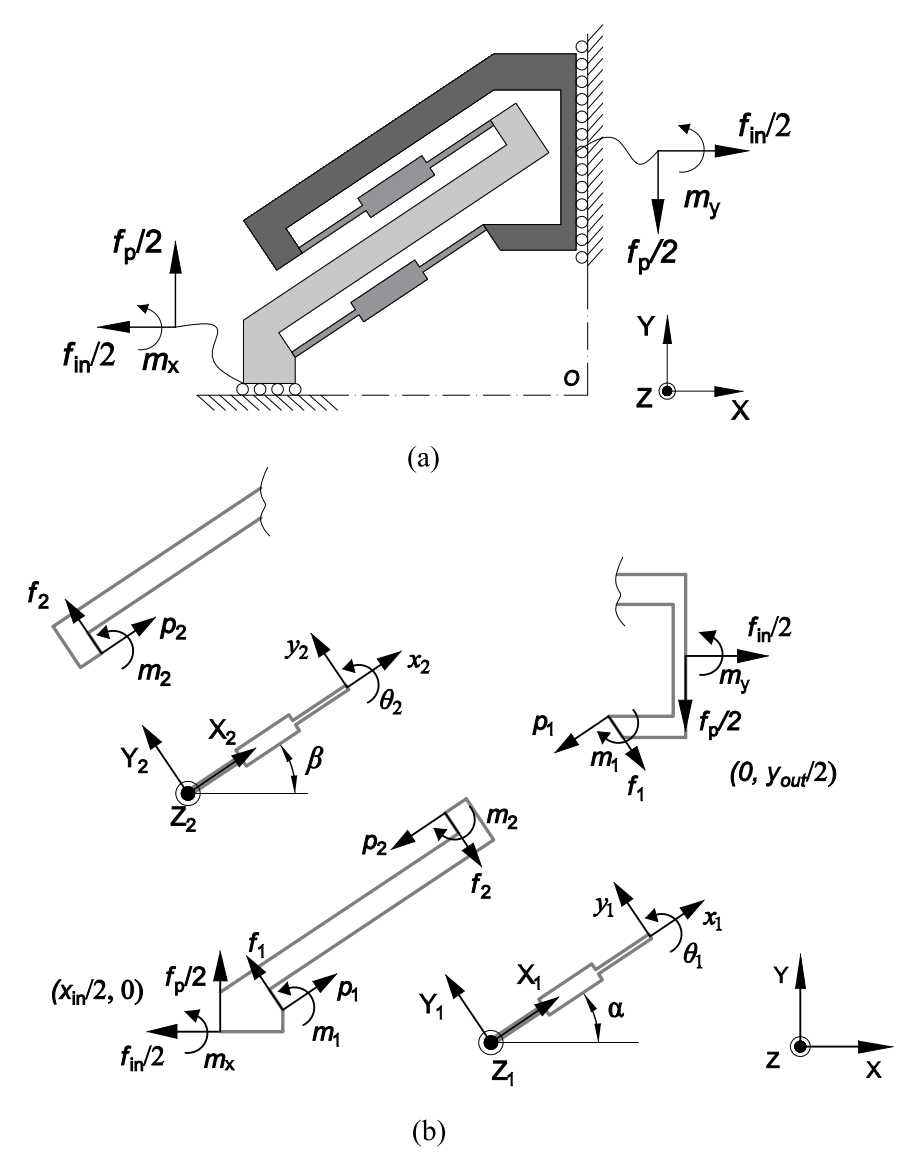


Fig. 5. The static modelling of a quarter of the amplifier: (a) a quarter of the OCARCM; (b) the FBD of the OCARCM.

$$\begin{cases} f_{\rm in}/2 + f_1 \sin\alpha - f_2 \sin\beta - p_1 \cos\alpha + p_2 \cos\beta = 0\\ -f_{\rm p}/2 - p_1 \sin\alpha + p_2 \sin\beta - f_1 \cos\alpha + f_2 \cos\beta = 0\\ m_{\rm y} - m_1 + m_2 - f_{\rm in}(b + h/2)/2 - f_1 b \sin\alpha + f_1 \cos\alpha(d - l\cos\alpha) + p_1 b \cos\alpha + p_1 \sin\alpha(d - l\cos\alpha)\\ + f_2 \sin\beta(c - l\sin\beta) - f_2 d\cos\beta - p_2 \cos\beta(c - l\sin\beta) - p_2 d\sin\beta = 0 \end{cases}$$
(5)

$$\begin{cases}
-f_{\rm in}/2 + f_2 \sin\beta - f_1 \sin\alpha - p_2 \cos\beta + p_1 \cos\alpha = 0 \\
f_p - f_2 \cos\beta + f_1 \cos\alpha - p_2 \sin\beta + p_1 \sin\alpha = 0 \\
m_x + m_1 - m_2 + f_1 d/2 - f_1 d\cos\alpha + f_1 \sin\alpha(b - l\sin\alpha) - p_1 \cos\alpha(b - l\sin\alpha) - p_1 d\sin\alpha - f_2 c\sin\beta \\
+ f_2 \cos\beta(d - l\cos\beta) + p_2 \cos\beta + p_2 \sin\beta(d - l\cos\beta) = 0
\end{cases}$$
(6)

The conditions of the geometric compatibility of the amplifier are given by,

$$\begin{cases} x_1 = -\frac{1}{2} y_{\text{out}} \cos \alpha + \frac{1}{2} x_{\text{in}} \cos \alpha \\ y_1 = -\frac{1}{2} y_{\text{out}} \cos \alpha - \frac{1}{2} x_{\text{in}} \sin \alpha \end{cases}$$

$$(7)$$

$$\begin{cases} x_2 = -\frac{1}{2}x_{\text{in}}\cos\beta + \frac{1}{2}y_{\text{out}}\sin\beta \\ y_2 = \frac{1}{2}x_{\text{in}}\sin\beta + \frac{1}{2}y_{\text{out}}\cos\beta \end{cases}$$
(8)

By solving the constitutive equations, load equilibrium and geometric compatibility equations simultaneously, one can obtain the displacements and amplification ratio as functions of applied forces. The analytical models for the general case of $\alpha \neq \beta$ are too complex to be presented here, which is graphically analyzed in Section 4 instead. While the models for the case when the beam slope $\alpha = \beta$ are presented below.

$$\begin{cases} x_{\rm in} = \frac{-3S^{1/3} f_{\rm p} k_5 \sin\alpha \cos\alpha + 3S^{1/3} f_{\rm in} k_5 (\cos\alpha)^2 - 48k_1 k_{33} \sin\alpha \cos\alpha + 2S^{2/3} \tan\alpha}{6k_{33}k_5 S^{1/3}} \\ y_{\rm out} = \frac{-3S^{1/3} f_{\rm in} k_5 \sin\alpha \cos\alpha - 3S^{1/3} f_{\rm p} k_5 (\cos\alpha)^2 - 48k_1 k_{33} (\cos\alpha)^2 + 3S^{1/3} f_{\rm p} k_5 + 2S^{2/3}}{6k_{33}k_5 S^{1/3}} \\ A_{\rm m} = \frac{-3S^{1/3} f_{\rm in} k_5 \sin\alpha \cos\alpha - 3S^{1/3} f_{\rm p} k_5 (\cos\alpha)^2 - 48k_1 k_{33} (\cos\alpha)^2 + 3S^{1/3} f_{\rm p} k_5 + 2S^{2/3}}{-3 \sin\alpha \cos\alpha S^{1/3} f_{\rm p} k_5 + 3S^{1/3} f_{\rm in} k_5 (\cos\alpha)^2 - 48k_1 k_{33} \sin\alpha \cos\alpha + 2S^{2/3} \tan\alpha} \end{cases}$$

$$(9)$$

where

$$S = 6 \sqrt{3} \sqrt{-27 \left(k_5^2 k_{33} \left(f_{\text{in}} + f_p\right) \left(f_{\text{in}} - f_p\right) \left(\cos\alpha\right)^2 - 2f_{\text{in}} f_p k_5^2 k_{33} \cos\alpha \sin\alpha - f_{\text{in}}^2 k_5^2 k_{33} - \frac{128 k_1^3}{27}\right) k_{33}^3 (\cos\alpha)^6} + 54 k_5 k_{32}^2 (\cos\alpha)^3 \left(f_{\text{in}} \sin\alpha + f_n \cos\alpha\right)$$

Furthermore, Eq. (9) can be simplified by dropping out some insignificant terms for an approximate calculation:

$$\begin{cases} x_{\rm in} \approx -\frac{\tan\alpha \left(24(\cos\alpha)^2 k_{11}^{(0)} k_{33} - S^{2\beta}\right)}{3k_{33}k_{11}^{(1)} S^{1\beta}} \\ y_{\rm out} \approx -\frac{24 (\cos\alpha)^2 k_{11}^{(0)} k_{33} - S^{2\beta}}{3k_{33}k_{11}^{(1)} S^{1\beta}} \\ A_{\rm m} = \frac{y_{\rm out}}{x_{\rm in}} \approx \frac{1}{\tan\alpha} \end{cases}$$

$$(10)$$

During the calculations for the amplification ratio (A_m), high-order terms are dropped without significantly affecting the accuracy of the results. The maximum error that results from dropping these high-order terms is less than 1.1%. Eq. (10) shows that the amplification ratio can be approximated by $1/\tan\alpha$ (α is the initial angle). This indicates that the amplification ratio over the whole range of motion is primarily determined by the flexure beam slope and is much less influenced by the input force and payload.

A comparison will be made between the amplification ratio characteristics of the OCARCM and those of the bridge-type compliant amplifier using the analytical model and FEA simulation. The main comparison variables are the different amplification ratios (by changing α and β), the different input and output forces, and the different beam stiffness (by changing A). The analytical model of the bridge-type compliant amplifier can be easily found by following the above derivation process.

4. Characteristics analysis with FEA verification

We compare and analyze the performance of the OCARCM from multiple perspectives. A study of the OCARCMs with different generic flexure beam slopes was undertaken in an effort to understand how slope affects the force-displacement characteristics and amplification ratio. A comparison of the OCARCM and the bridge-type amplifiers with the same generic flexure beam slope was conducted. The case where the OCARCMs were assigned payload (F_L) was analyzed to examine their performance in response to the loading. Furthermore, the case where the lumped-compliance (a=1/3) and distributed-compliance (a=1/2) OCARCM is also considered. All the designs were modeled in COMSOL@5.0 using identical flexure beam parameters listed in Table 1. The simulation assumes that the stages and base set are rigid, similar to the assumptions made in analytical modeling. Nonlinear solvers were used since there are large elastic deformations. Finer hexahedra mesh was generated at the flexure beam to gain stable and accurate results. The aluminum alloy AL6061 with Young's Modulus 69 GPa and Yield Strength 276 MPa was assigned to the material. A series of incremental forces or displacements were applied to the input stages during the simulation. All the parameters were switched back to

Table 1Parameters for all the cases in this section.

L	U	T	A	
30 mm	8 mm	0.8 mm	Lumped-compliance: 5 mm and 10 mm	Distributed-compliance: 15 mm

dimensional values for a more straightforward comparison.

Fig. 6(a) plots the exaggerated results of applying 0.4 mm displacement at each input stage. The resultant displacement of the OCARCM is about 1.39 mm, while the displacement of the bridge-type amplifier is 1.44 mm. The reduced displacement of the OCARCM reveals the over-constrained behavior occurring in the output stage.

The force-displacement relationship of both lumped-compliance and distributed-compliance OCARCMs are plotted in Fig. 7. The plot reveals a good correlation between FEA and analytical results, where the maximum error is less than 1.0%, and it also shows that the OCARCM with a larger flexure beam slope has larger stiffness. It can be observed in both analytical and FEA results that the force-displacement characteristic shows nonlinear characteristics, which are not encompassed by linear models.

In Fig. 8, we compared the amplification of the lumped-compliance (A=5 mm, A=10 mm) and the distributed-compliance (A=15 mm) OCARCMs to that of the lumped-compliance and distributed-compliance bridge-type amplifiers, respectively. It is worth noting that the amplification ratio is obtained based on Eq. (9). In the case of a zero-input displacement ($x_{\rm in}$), the amplification ratio is not captured, since division by zero is mathematically undefined. In his way, the plots for the amplification ratio are not continuous lines. The plots reveal that the amplification ratio of the bridge-type compliant amplifier varies with the input displacement at a large scale while that of the OCARCM shows a nearly constant amplification ratio for both the lumped-compliance design and the distributed-compliance design. Both FEA and analytical results show that the amplification ratio of the proposed OCARCM decreased by 1% while the bridge-type amplifier decreased by 13.9% for the design with the same flexure beam slope ($\alpha=\beta$) of 15°. Moreover, the amplification ratio of the OCARCM is close to the simplified analytical expression ($A_{\rm m}=1/\tan\alpha$), especially when the displacement is small. The maximum error occurs in Fig. 8(d) where the amplification ratio of the OCARCM is 1.73% smaller than the simplified results (the red dash-dot line).

It is also worth noting that there is a relatively larger nonlinearity in the amplification ratio of the design with a beam slope of 15^0 compared to the ones with 30^0 and 45^0 . The nonlinear effect of load-stiffening and elastokinematic nonlinearities can be seen in Eqs. (2) and (3) which are associated with the axial load p. The nonlinear effects are significant for the OCARACM with a smaller beam slope as the proportional force of the input force in the axial direction imposed on each flexure beam is large. Thus, the amplification ratio of the design with a smaller beam slope produces a larger nonlinear effect.

The effect of the payload (F_L) on the amplification ratio is illustrated in Fig. 9. Fig. 9(a) presents the amplification ratio of the lumped-compliance OCARCM (A=10 mm, $\alpha=\beta=15^0$) in response to different payloads. The results obtained from the FEA show good agreement with those obtained from the analytical results with a maximum error of 0.72%. The amplification ratio of the lumped-compliance OCARCM varies between 3.56 and 3.83 at small input as the payload changes from -40 N to 40 N.

The amplification ratio of the bridge-type amplifier in response to the payload is graphically shown in Fig. 9(b). The FEA results are consistent with the analytical results. Both results indicate that the amplification ratio of the bridge-type amplifier changes at a large scale, ranging from 3.25 to 4.54. However, the variation of the amplification ratio is not only contributed by the payload but also by the character of the bridge-type amplifier itself. To demonstrate the effect of the payload on the amplification ratio, we plot the variation of the amplification ratio of the OCARCM and bridge-type amplifier in response to different payloads ranging from – 40 N to 40 N in Fig. 9 (c). The amplification ratio of the bridge-type amplifier varies within the orange region which is much larger than that of the blue region. This means the amplification ratio of the OCARCM is more robust to the applied payload. Both types of amplifiers also present the trend that the larger the payload, the greater the variation in the amplification ratio.

The comparison between the amplification ratio of the lumped-compliance (relatively high stiffness) and the distributed-compliance (relatively high compliance) is plotted in Fig. 10. The amplification ratio of the distributed OCARCM varies between 3.54 and 3.87, while the amplification ratio of the lumped-compliance OCARCM varies between 3.56 and 3.83 as the payload changes from – 40 N to 40 N. This indicates that the amplification ratio of the lumped-compliance OCARCM is more robust to the payload compared with distributed-compliance OCARCM. Another pattern we can observe from the plot is that the stiffness has a slight

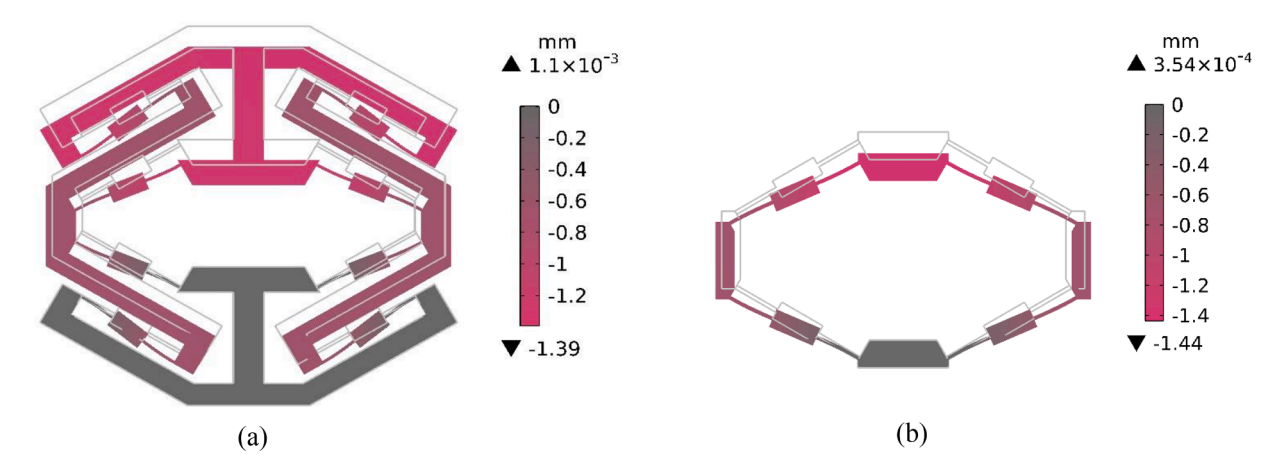


Fig. 6. Displacement analysis: (a) the exaggerated view of the displacement plot of the OCARCM with the flexure beam slope of 30°; (b) the deformation of the corresponding bridge-type amplifier.

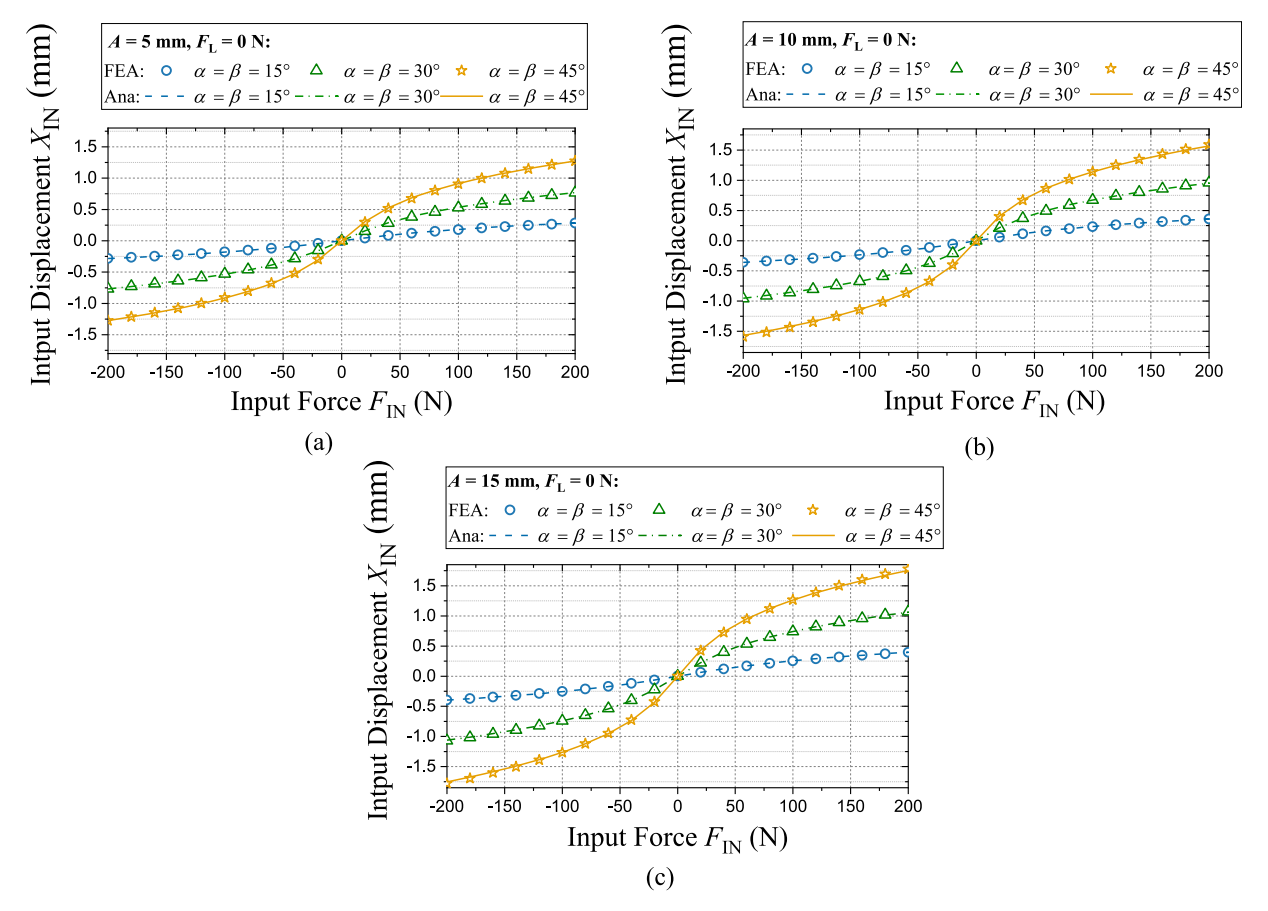


Fig. 7. Force-displacement characteristics without payload ($F_L = 0$): (a) lumped-compliance (A = 5 mm); (b) lumped-compliance (A = 10 mm); (c) distributed-compliance (A = 15 mm).

influence on the variation scale of the amplification ratio. The difference is below 1.62% between the lumped-compliance OCARCM and the distributed-compliance OCARCM.

The influence of the different beam slopes ($\alpha \neq \beta$) on the amplification ratio is also investigated and plotted in Fig. 11. A decrease in the amplification ratio first can be observed as the difference between the two flexure beams' slopes increases. With an increased slope difference (α minus β), the design also shows a more linear trend and a greater change in amplification ratio as the input displacement gradually increases. It tends to be preferable to design flexure beams with the same slope since it exhibits less deviation of the amplification ratio than those with different slopes.

5. Experiment tests

The prototype with distributed-compliance is selected as the candidate to obtain experimental results, which can verify the FEA and analytical results. The compliant loading spring is selected as the payload to mimic the actuation of compliant mechanisms. These experiments are less investigated but are becoming more popular as compliant mechanisms become more widely used. The influence of the loading spring on the force-displacement characteristics and the amplification ratio of the OCARCM is analyzed and discussed in the following sections.

5.1. Fabrication of the OCARCM prototype

The prototype (Fig. 12(b)) is monolithically manufactured using a computer numerical control (CNC) milling machine from a piece of AL7075 plate, using the same parameters listed in Table 1. The AL7075 material with Young's modulus of 71 GPa was selected due to its lightweight and high-yield stress. A $1.5 \, \text{mm}$ radius fillet corner is created by the milling tools. To avoid the deformation of the thin beam (0.8 mm), 3D-printed blocks are embedded to support the beams while machining. The overall dimension of this OCARCM prototype is $195 \, \text{mm} \times 160 \, \text{mm} \times 10 \, \text{mm}$.

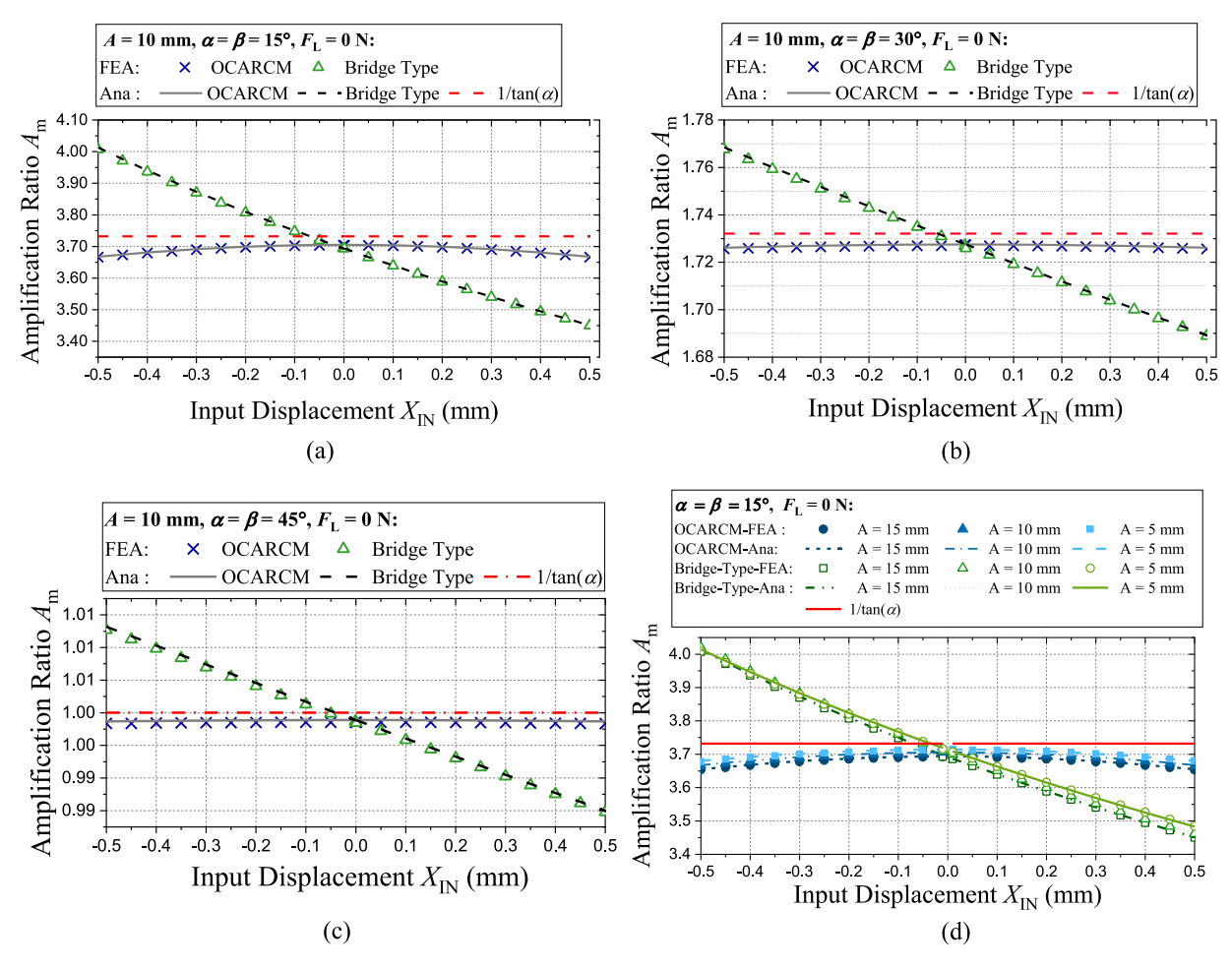


Fig. 8. Comparison between bridge-type amplifier and OCARCM with the equal beam slope ($\alpha = \beta$): (a) lumped-compliance (A = 5 mm); (b) lumped-compliance (A = 10 mm); (c) distributed-compliance (A = 15 mm); (d) OCARCM compared with the bridge-type compliant amplifier with different compliance.

5.2. Experimental setup

Loading springs were used to mimic the payload of the OCARCM, which is fabricated using 3D printing. Their stiffness was tested with a stiffness of 3.67 N/mm for loading stiffness 1 and a stiffness of 9.47 N/mm for load stiffness 2. The stiffness testing rig is shown in Fig. 12(a). The motion range of the loading spring is designed to be 6 mm which satisfies the output displacement demand of the OCARCM. The force sensor and the micrometer are utilised to measure the reaction force and the input displacement, respectively.

Fig. 12(c) shows the experimental setup of the OCARCM with a spring payload. In typical cases, a piezoelectric actuator is employed to achieve displacement amplification in the amplifier. However, in this particular experiment, we opted to use a pulley system and weights as our actuators. By using the pulley system, we were able to simulate bidirectional input forces (against the PZT's unidirectional actuation), allowing us to fully characterize the properties of the OCARCM. Previously, the OCARCM was actuated by giving forces to both input stages, as illustrated in Fig. 3. It was difficult to use a pulley system to actuate both input stages simultaneously with an even actuation force given to each input stage. Therefore, we fixed one of the input stages as the base, and the other input stage connects to the pulley system, as shown in Fig. 12(b) and (c). During the experiment, a pair of identical springs (loading spring 2) was installed on the top and bottom surfaces of the OCARCM to avoid the introduction of an out-of-plane payload. Dial gauges were used to measure the displacement of both the input and output stages, with a motion resolution of 0.001 mm and a spring force of 0.4–0.7 N. The OCARCM was actuated by applying a fixed force interval ranging from 0 to 200 N, and the corresponding dial gauge output displacements were recorded for each step. The experimental procedure was repeated three times to obtain an average result for each force interval.

5.3. Experimental results

The experiment has been conducted to validate the FEA and analytical results. Fig. 13(a)-(c) plot the input force versus the input

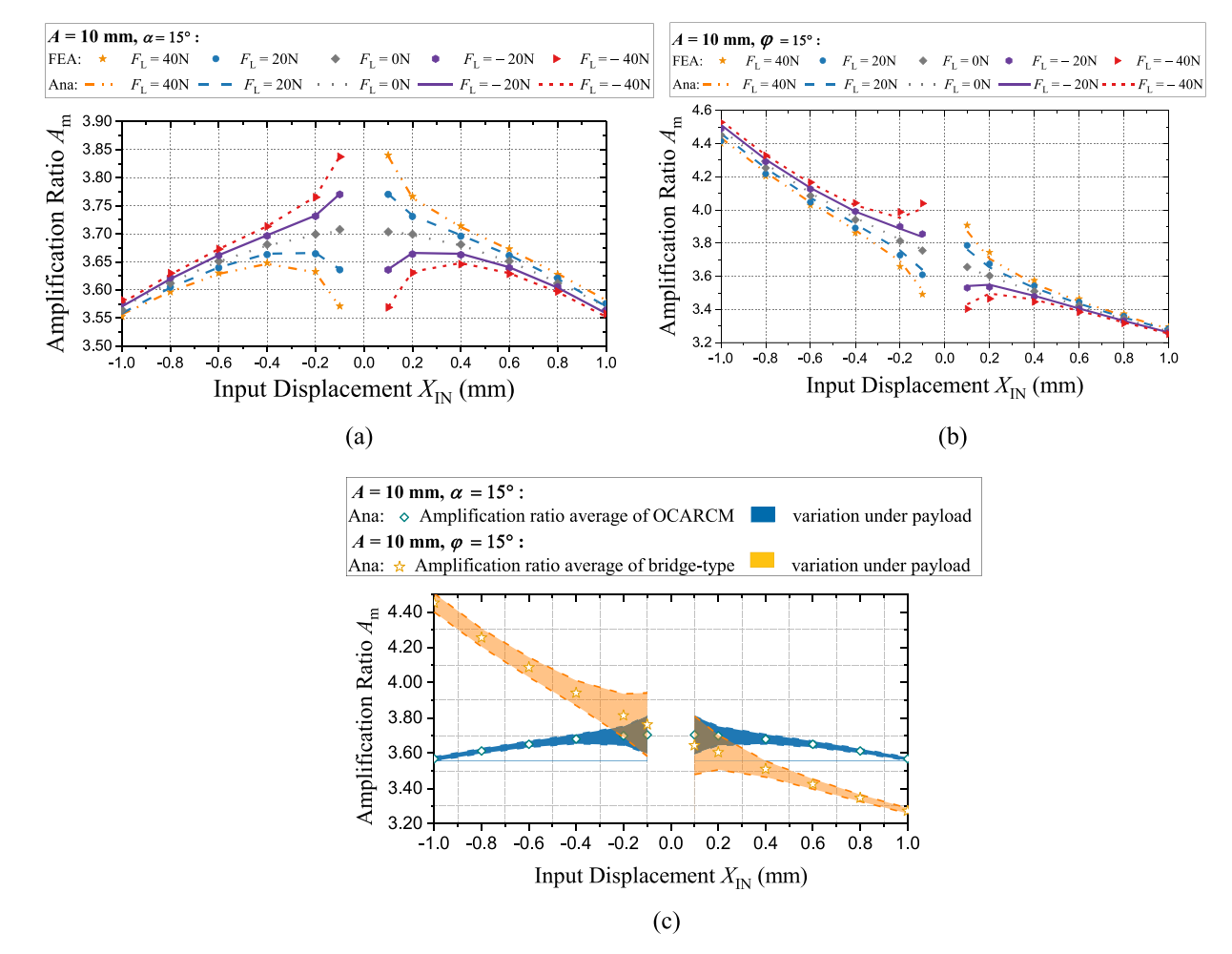


Fig. 9. The amplification ratio under different payloads F_L : (a) the FEA results of the OCARCM compared with its analytical results; (b) the FEA results of the bridge-type compliant amplifier compared with its analytical results; (c) variation of the amplification ratio in response to the different payload F_L .

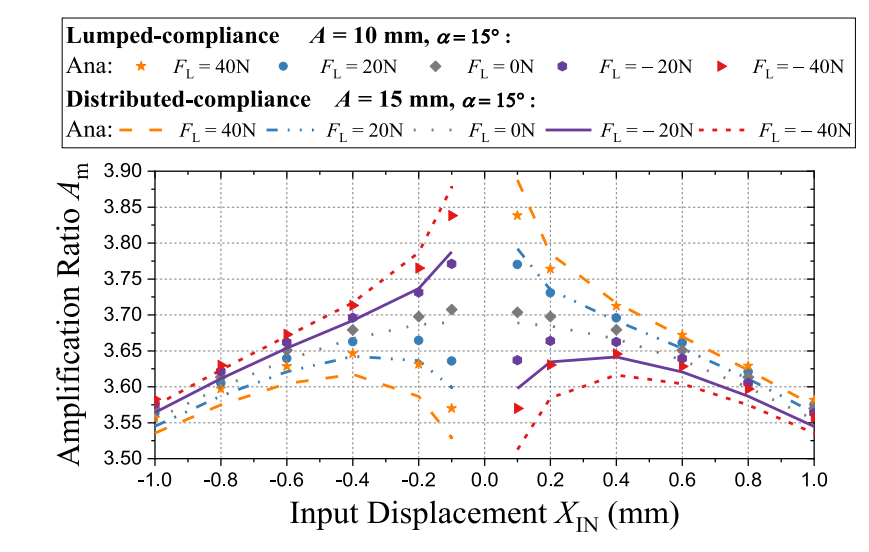


Fig. 10. The comparison between the lumped-compliance and the distributed-compliance under different payloads $F_{\rm L}$.

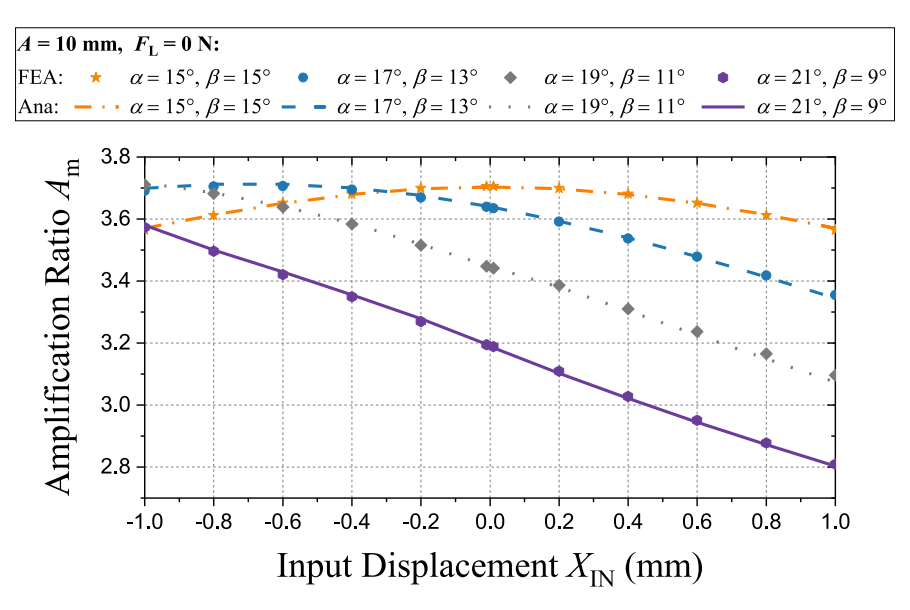


Fig. 11. Amplification ratio of the lumped-compliance OCARCM with different beam slopes ($\alpha \neq \beta$).

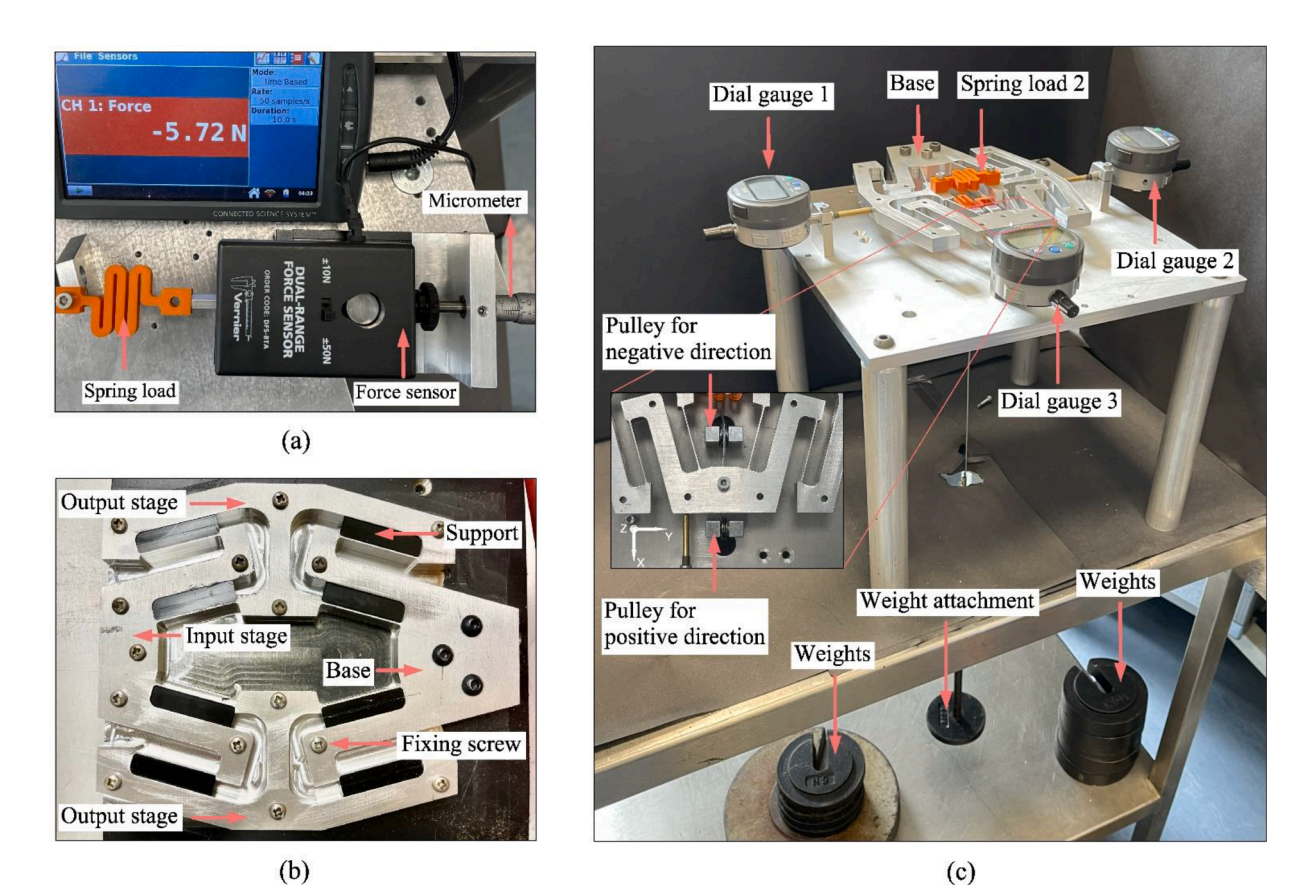


Fig. 12. Prototype and experiment setup of the OCARCM: (a) testing of loading spring; (b) monolithically fabricated; (c) assembly.

displacement with different loading springs. The FEA results show good agreement with the analytical results. And both results show a nonlinear pattern. In contrast, the experiment results generally show a linear pattern compared to the FEA results or analytical results. Fig. 13(d) presents the error/discrepancy between the experimental results and analytical results with a maximum error of 14.5%. The error for the case with the loading spring is much larger than that for the case without the loading spring over the motion range close to

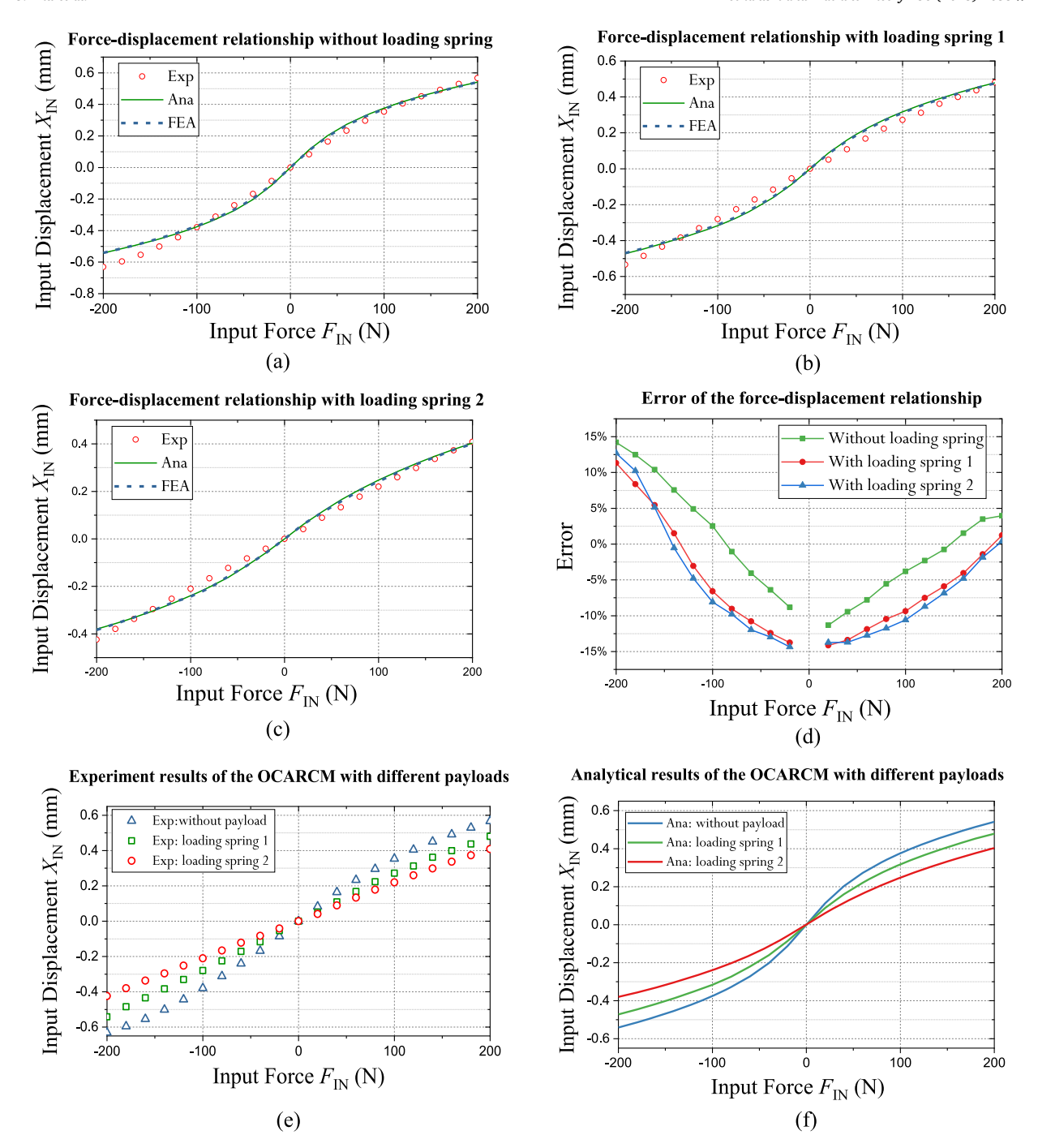


Fig. 13. Force-displacement relationship: (a) without loading spring; (b) with loading spring 1; (c) with loading spring 2; (d) the error between experimental and analytical results; (e) integrated plots of experiment results; (f) integrated plots of analytical results.

the home position (zero input). This discrepancy could be attributed to the deformation of the parts, such as the output stage and input stage, which were assumed to be rigid in the analytical mode. Additionally, it can occur due to the assembly error of the test rig. For instance, a small misalignment between the string in the pulley system and the mechanism's symmetric line may cause uneven displacement between the two-output stages. Fig. 13(e) and (f) presents the experiment results and analytical results of the force-displacement characteristics of the OCARCM with and without payload, respectively. These plots indicate that the stiffness of the OCARCM increases as we increase the stiffness of the loading spring. This is also called the load-dependent effect. Furthermore, the pattern of the force-displacement relationship turns out to be more linear as we increase the stiffness of the loading spring. This, as aforementioned, can be caused by the deformation of the parts assumed to be rigid.

Hereafter we analyzed the influence of the loading spring on the amplification ratio of the OCARCM as shown in Fig. 14. The experiment results generally show a constant value with small fluctuations. While the FEA and analytical results show a small increase trend and a decreasing trend. However, the variation in amplification ratio is very small (below 2.1% in experiment results and below 0.67% in FEA and analytical results). As the stiffness of the loading spring increases, the OCARCM amplification ratio falls. The error bar in Fig. 14(a)–(c) illustrates the standard deviation of the three-time experiment results. The standard deviation of the experiment without payload is generally smaller than the ones with payload. Several factors contribute to this, including the assembly of the loading spring and the low repeatability of the 3D-printed loading spring. The error between the experimental results and the analytical results is plotted in Fig. 14(d). The plot shows a fluctuation pattern with a relatively low maximum error of 3.4%. The amplification ratio is dominated by the flexure beam slope. So, manufacturing errors such as the variation of the beam thickness or beam length will not have a noticeable contribution to the amplification ratio error.

6. Further discussions

6.1. Dynamic performance

A modal analysis was conducted to gain insight into the dynamic behavior of the OCARCM, and the results of which were compared with those of a corresponding bridge-type amplifier. Using FEA, we obtained the first-four modes of both the bridge-type amplifier and the OCARCM as shown in Fig. 15. The results showed that the first two modes of the OCARCM occur at 142.3 Hz and 191.9 Hz, corresponding to the output stage translations along the Y-axis (desired output direction) and X-axis, respectively. The third mode is the output stage rotation about X-axis and the fourth mode is the output stage rotation about the Z-axis at a large natural frequency of 1378 Hz. In contrast, the first mode of the bridge-type compliant amplifier is the translation of the output stage in the X-direction (undesired output direction) at a natural frequency of 117.6 Hz. The second mode of the bridge-type amplifier is the output stage translation along the Y-axis. The third and fourth modes of the bridge-type amplifier are the output stage rotations about the X-axis and

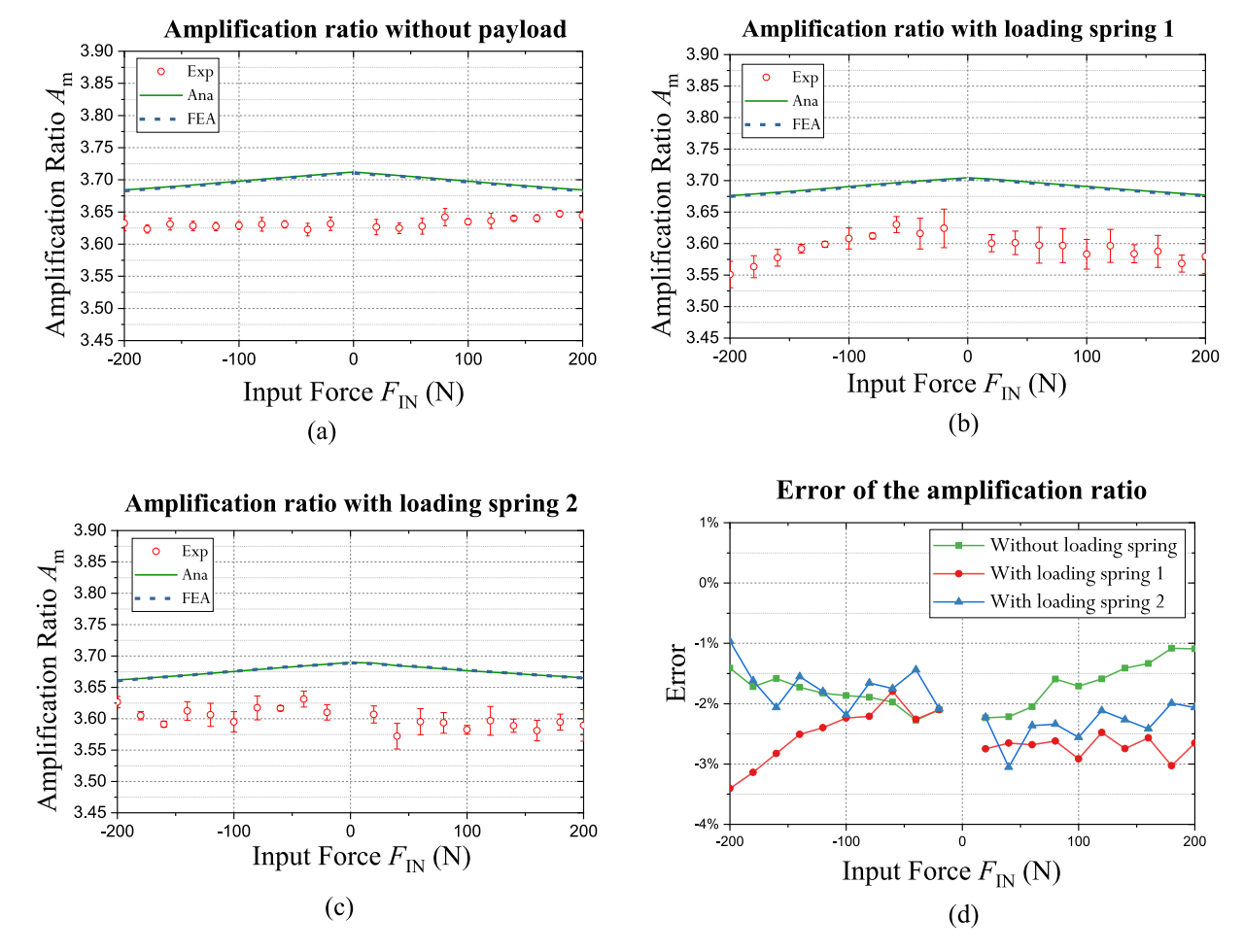


Fig. 14. Amplification ratio of the OCARCM with different loading springs: (a) amplification ratio without payload; (b) amplification ratio with loading spring 1; (c) amplification ratio with loading spring 2; (d) Error between the experimental results and analytical results.

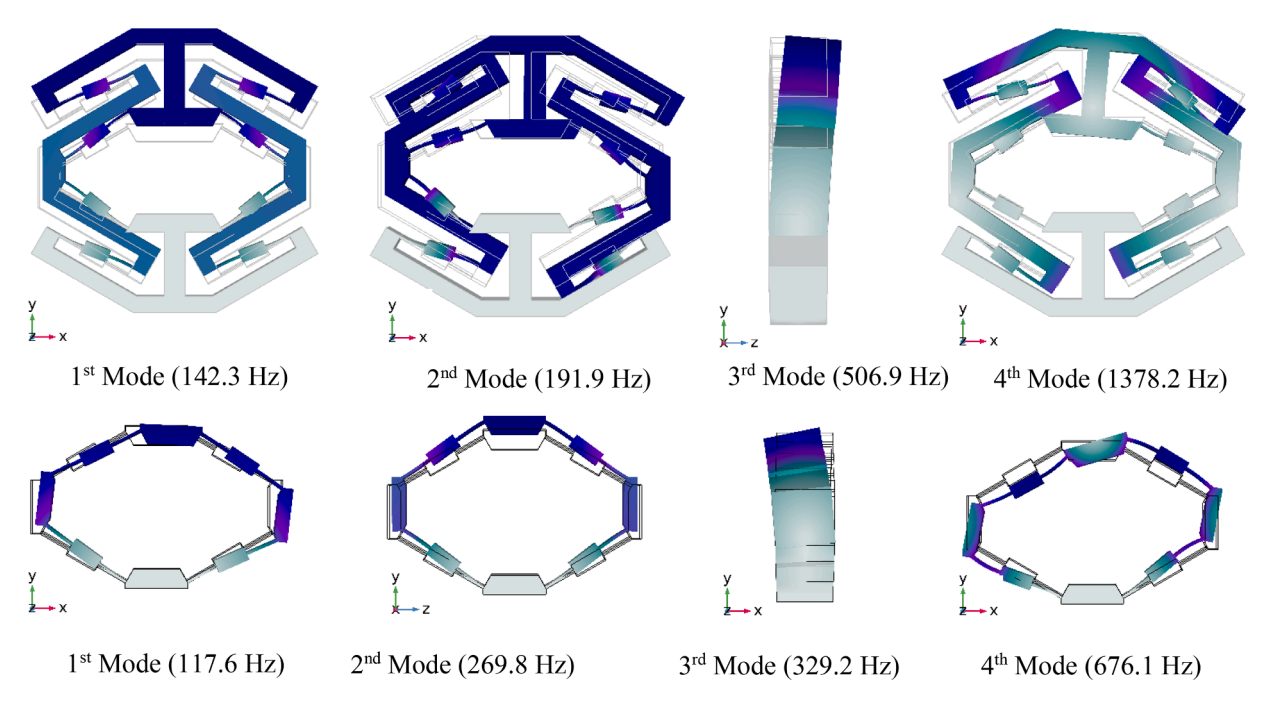


Fig. 15. The first-four natural frequencies.

the Z-axis, at a natural frequency of 329.2 Hz and 676.1 Hz, respectively.

The output stage of the OCARCM is much heavier than that of the bridge-type amplifier. This leads to a relatively low natural frequency in the OCARCM's Y-direction (1st mode) compared to the natural frequency in the bridge-type amplifier's Y-direction (2nd mode). However, other frequencies of the OCARCM are higher than those of the bridge-type amplifier. For example, the natural frequency of the output stage rotation about the Z-axis (4th mode: 1378.2 Hz) is twice that of the bridge-type amplifier (4th mode: 676.1 Hz), because the in-plane rotation of the output stage of the OCARCM is better constrained than that of the bridge-type amplifier due to our new over-constraint design approach. Additionally, the rotation of the input stage of the bridge-type amplifier is also observed in the 1st mode (117.6 Hz), while the rotation of the input stage of the OCARCM happens at the 4th mode (1378.2 Hz). These findings suggest that both the output stage and the input stage of the OCARCM are less susceptible to rotational oscillations. While the OCARCM has a low 1st mode natural frequency in the Y-direction, this can potentially be improved through mass optimization of the output stage.

6.2. Eliminating force-displacement nonlinearity

Over-constraint based design method mitigates variations in amplification ratios and increases robustness to payload variations. This may adversely lead to a nonlinear force-displacement relationship (load-stiffening effect) when using straight flexure beams as observed in Fig. 13. This nonlinear effect is not desired for a very large range of motion and a small actuation effort [12,54]. To eliminate the force-displacement nonlinearity, a potential solution is presented in Fig. 16(a). Under the same topology, the straight beams were replaced by the Z-shape beams to alleviate the force-displacement nonlinearity.

The deformed configuration obtained from the FEA simulation is shown in Fig. 16(b). The FEA shows a linear pattern between the force and displacement which is desired. We also compared the amplification ratio between the bridge-type compliant amplifier, OCARCM with straight beams and OCARCM with Z-shape beams. The dominant factor that influences the value of the amplification ratio is the slope of the flexure beam. This also applies to OCARCM with Z-shape beams. The angle of the endpoints of the Z-shape beams is set as 12.5° and corresponds to an amplification ratio of 2.95. And the angle of the straight beam in both bridge-type compliant amplifiers and the original OCARCM is set as 18.73° to produce the same amplification ratio. The OCARCM with Z-shape beams shows a similar pattern as OCARCM with straight beams (previous design) but has a relatively larger variation in amplification ratio as depicted in Fig. 17(b). And the bridge-type amplifier still shows a large variation in amplification ratio.

6.3. Reducing the footprint

Compared to the bridge-type compliant amplifier, the footprint of the OCARCM increases due to the added extra flexure beams. This may bring a drawback in certain applications where space is limited. To address this issue, a multi-layer design method can be implemented [55,56]. As presented in Fig. 18(a), it shows a three-layer design with a reduced footprint. Fig. 18(b) shows the deformed shape of the three-layer design. The footprint has been significantly reduced in comparison to the planar OCARCM, However, it

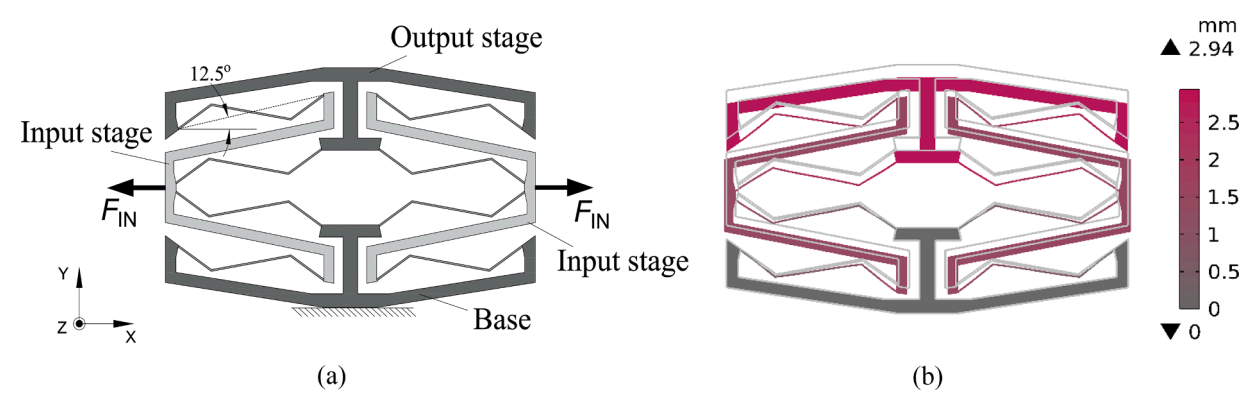


Fig. 16. (a) OCARCM with Z-shape beams; (b) its deformed configuration.

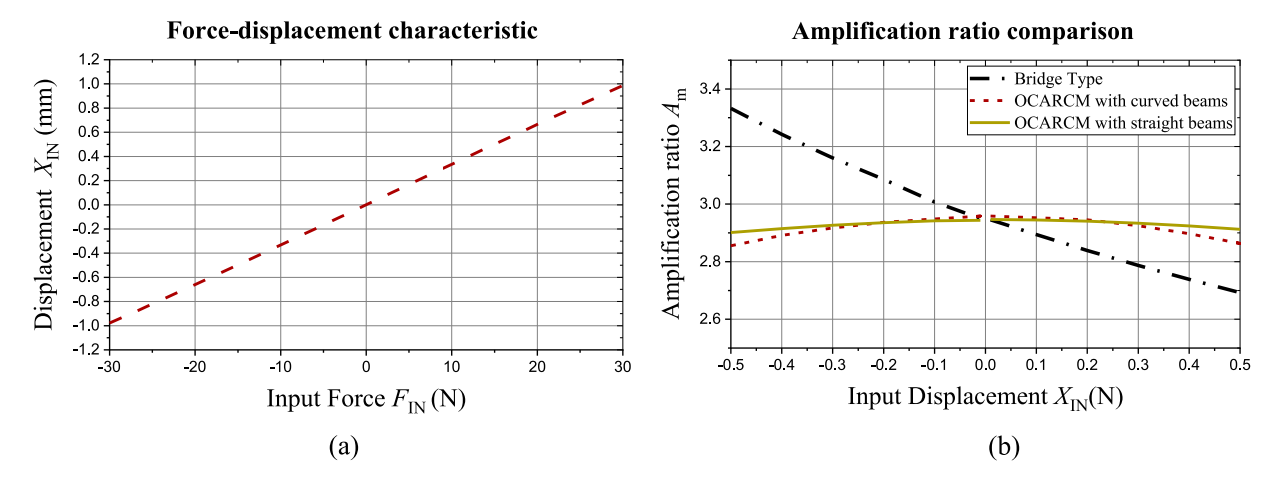


Fig. 17. Nonlinear FEA results: (a) force-displacement plot; (b) amplification ratio comparison.

simultaneously increases the difficulty of fabrication. The tradeoff between footprint and manufacturing complexity should be taken into account during practical applications.

7. Conclusion

A compliant amplifier with a constant amplification ratio was designed to allow a uniform output motion resolution/precision. The proposed OCARCM is compared to a commonly used bridge-type compliant amplifier in terms of its ability to maintain a constant amplification ratio with and without payload. A free-body diagram (FBD) and beam constraint model (BCM) are used to obtain closed-form solutions that reveal nonlinearities in the force-displacement characteristics of the OCARCM. A prototype is fabricated and tested to validate the force-displacement and amplification ratio characteristics of the OCARCM. COMSOL with large deformation turned on was used for nonlinear FEA analysis to corroborate the analytical modeling. Based on the discussions, the main contribution of this paper can be summarized below:

- (1) A compliant amplifier with a nearly constant amplification ratio allows a uniform output motion resolution/precision.
- (2) The closed-form solutions are developed which can accurately quantify the force-displacement characteristics and amplification ratio of the proposed OCARCM.
- (3) The FEA results based on the COMSOL show good agreement with the closed-form solutions with a maximum error of 1%, even in the case of large deformation.
- (4) An experiment was set up based on a CNC-machined aluminum prototype. The experimental results showing the variation of the amplification ratio is below 2.1% with loading springs. And the error between the experiment results and FEA or analytical results is below 3.4% within the output motion range of 1.76 mm.

It is possible to address the issues existing in the OCARCM, including its nonlinear force-displacement characteristic and relatively large footprint, by using the methods in Section 6.

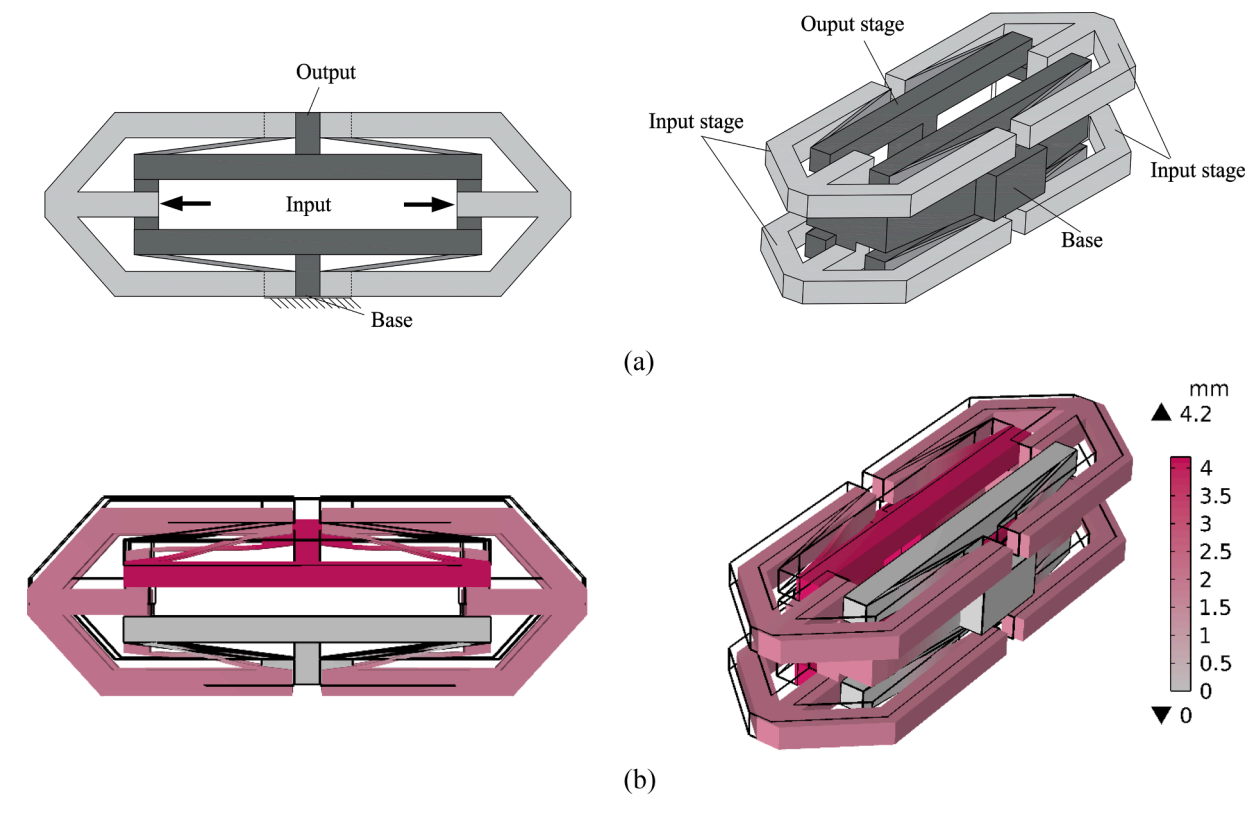


Fig. 18. Three-layer design with reduced footprint: (a) geometry of the design; (b) deformed configuration.

Declaration of Competing Interest

The authors declare that they have no known competing financial interests or personal relationships that could have appeared to influence the work reported in this paper.

Data availability

Data will be made available on request.

Acknowledgments

Jiaxiang Zhu is grateful for the financial support from the China Scholarship Council (CSC Student ID: 202008300013). Haiyang Li is thankful to the National Natural Science Foundation of China (No. 51975108). The authors also would like to greatly acknowledge Mr. Tomothy Power and Mr. Michael O'Shea for their help in the fabrication of the prototype.

References

- $[1] L.L.\ Howell,\ Compliant\ mechanisms.\ 21st\ Century\ Kinematics,\ Springer,\ 2013,\ pp.\ 189-216,\ https://doi.org/10.1007/978-1-4471-4510-3_7.$
- [2] N. Lobontiu, Compliant Mechanisms: Design of Flexure Hinges, CRC press, 2002, https://doi.org/10.1201/9781420040272.
- [3] M. Hamedi, P. Salimi, M. Vismeh, Simulation and experimental investigation of a novel electrostatic microgripper system, Microelectron. Eng. 98 (2012) 467–471, https://doi.org/10.1016/j.mee.2012.07.096.
- [4] G. Deng, N. Wang, C. Zhou, J. Li, A simplified analysis method for the Piezo Jet dispenser with a diamond amplifier, Sensors 18 (7) (2018) 2115, https://doi.org/10.3390/s18072115.
- [5] Zhou, S., and Yan, P., 2023, Design and analysis of a hybrid displacement amplifier supporting a high-performance Piezo Jet dispenser, 14 (2), pp. 322.
- [6] F. Qian, T.B. Xu, L. Zuo, Piezoelectric energy harvesting from human walking using a two-stage amplification mechanism, Energy 189 (2019), https://doi.org/10.1016/j.energy.2019.116140.
- [7] M.A. Abdelnaby, M. Arafa, Energy harvesting using a flextensional compliant mechanism, J. Intell. Mater. Syst. Struct. 27 (19) (2016) 2707–2718, https://doi. org/10.1177/1045389x16641220.
- [8] M.M. Elsisy, M.H. Arafa, C.A. Saleh, Y.H. Anis, Modeling of a symmetric five-bar displacement amplification compliant mechanism for energy harvesting, Sensors 21 (4) (2021) 1095, https://doi.org/10.3390/s21041095.
- [9] X. Chen, Y. Li, Design, modeling and testing of a vibration absorption device with energy harvesting based on force amplifier and piezoelectric stack, Energy Convers. Manage. 255 (2022), https://doi.org/10.1016/j.enconman.2022.115305.

- [10] H. Wu, L. Lai, L. Zhang, L. Zhu, A novel compliant XY micro-positioning stage using bridge-type displacement amplifier embedded with Scott-Russell mechanism, Precis. Eng. 73 (2022) 284–295, https://doi.org/10.1016/j.precisioneng.2021.09.014.
- [11] G. Hao, X. Kong, A novel large-range XY compliant parallel manipulator with enhanced out-of-plane stiffness, J. Mech. Des. 134 (6) (2012), https://doi.org/10.1115/1.4006653.
- [12] A. Bazaei, M.H. Ettefagh, Z. Chen, Displacement amplification and differential actuation in piezo driven nanopositioners, Mech. Syst. Signal Process. 151 (2021), 107356, https://doi.org/10.1016/j.ymssp.2020.107356.
- [13] X. Xi, T. Clancy, X. Wu, Y. Sun, X. Liu, A MEMSXY-stage integrating compliant mechanism for nanopositioning at sub-nanometer resolution, J. Micromech. Microeng. 26 (2) (2016), 025014, https://doi.org/10.1088/0960-1317/26/2/025014.
- [14] F. Wang, Z. Huo, C. Liang, B. Shi, Y. Tian, X. Zhao, D. Zhang, A novel actuator-internal micro/nano positioning stage with an arch-shape bridge-type amplifier, IEEE Trans. Ind. Electron. 66 (12) (2019) 9161–9172, https://doi.org/10.1109/tie.2018.2885716.
- [15] J. Chen, C. Zhang, M. Xu, Y. Zi, X. Zhang, Rhombic micro-displacement amplifier for piezoelectric actuator and its linear and hybrid model, Mech. Syst. Signal Process. 50-51 (2015) 580–593, https://doi.org/10.1016/j.ymssp.2014.05.047.
- [16] J.H. Kim, S.H. Kim, Y.K. Kwak, Development and optimization of 3-D bridge-type hinge mechanisms, Sens. Actuators A 116 (3) (2004) 530–538, https://doi.org/10.1016/j.sna.2004.05.027.
- [17] P. Liu, P. Yan, A new model analysis approach for bridge-type amplifiers supporting nano-stage design, Mech. Mach. Theory 99 (2016) 176–188, https://doi.org/10.1016/j.mechmachtheory.2016.01.005.
- [18] Slusher, R.B., and Westminster, C. 1999. Motion reducing flexure structure. U.S.Patent 5,969,892, Ball Aerospace & Technologies Corp., Broomfield, Colo.
- [19] Ling, M., Wang, J., Wu, M., Cao, L., Fu, B.J. S., and Physical, A.A., 2021, Design and modeling of an improved bridge-type compliant mechanism with its application for hydraulic piezo-valves, 324, pp. 112687.
- [20] X. Shen, L. Zhang, D. Qiu, A lever-bridge combined compliant mechanism for translation amplification, Precis. Eng. 67 (2021) 383–392, https://doi.org/10.1016/j.precisioneng.2020.10.010.
- [21] J. Qian, P. Yan, Design and analysis of a compliant micro-gripper with LBL type displacement amplifier, in: Proceedings of the IEEE International Conference on Manipulation, Manufacturing and Measurement on the Nanoscale (3M-NANO), 2019, pp. 112–117, https://doi.org/10.1109/3m-nano46308.2019.8947391.
- [22] G. Chen, Y. Ma, J. Li, A tensural displacement amplifier employing elliptic-arc flexure hinges, Sens. Actuators A 247 (2016) 307–315, https://doi.org/10.1016/j.
- [23] P.R. Ouyang, W.J. Zhang, M.M. Gupta, A new compliant mechanical amplifier based on a symmetric five-bar topology, J. Mech. Des. 130 (10) (2008), https://doi.org/10.1115/1.2965600.
- [24] J. Zhu, G. Hao, Design and test of a compact compliant gripper using the Scott–Russell mechanism, Arch. Civ. Mech. Eng. 20 (3) (2020), https://doi.org/10.1007/s43452-020-00085-3
- [25] H. Li, F. Guo, Y. Wang, Z. Wang, C. Li, M. Ling, G. Hao, Design and modeling of a compact compliant stroke amplification mechanism with completely distributed-compliance for ground-mounted actuators, Mech. Mach. Theory 167 (2022), 104566, https://doi.org/10.1016/j.mechmachtheory.2021.10456
- [26] M. Ling, C. Zhang, L. Chen, Optimized design of a compact multi-stage displacement amplification mechanism with enhanced efficiency, Precis. Eng. 77 (2022) 77–89, https://doi.org/10.1016/j.precisioneng.2022.05.012.
- [27] P. Prabhu, Muralidhara, R.K. Veeresha, T.R. Venugopal, Design, fabrication, and testing of flexurally amplified piezo actuator, Mater. Today Proc. 46 (2021) 9490–9497, https://doi.org/10.1016/j.matpr.2020.03.502.
- [28] Q. Xu, Y. Li, Analytical modeling, optimization and testing of a compound bridge-type compliant displacement amplifier, Mech. Mach. Theory 46 (2) (2011) 183–200, https://doi.org/10.1016/j.mechmachtheory.2010.09.007.
- [29] W. Chen, C. Kong, Q. Lu, Y. Liang, L. Luo, H. Wei, Nonlinear analysis, optimization, and testing of the bridge-type compliant displacement amplification mechanism with a single input force for microgrippers, Precis. Eng. 73 (2022) 166–182, https://doi.org/10.1016/j.precisioneng.2021.09.001.
- [30] H.W. Ma, S.M. Yao, L.Q. Wang, Z. Zhong, Analysis of the displacement amplification ratio of bridge-type flexure hinge, Sens. Actuators A 132 (2) (2006) 730-736, https://doi.org/10.1016/j.sna.2005.12.028.
- [31] K.B. Choi, J.J. Lee, G.H. Kim, H.J. Lim, S.G. Kwon, Amplification ratio analysis of a bridge-type mechanical amplification mechanism based on a fully compliant model, Mech. Mach. Theory 121 (2018) 355–372, https://doi.org/10.1016/j.mechmachtheory.2017.11.002.
- [32] J. Hricko, Š. Havlík, Compliant mechanisms for motion/force amplifiers for robotics, Advances in Service and Industrial Robotics: Proceedings of the 28th International Conference on Robotics in Alpe-Adria-Danube Region (RAAD 2019), Springer International Publishing. (2020) 26–33, doi:10.1007/978-3-030-19648-6 4.
- [33] F. Chen, Q. Zhang, Y. Gao, W. Dong, A review on the flexure-based displacement amplification mechanisms, IEEE Access 8 (2020) 205919–205937, https://doi. org/10.1109/access.2020.3037827.
- [34] B.J. Pokines, E.J. Garcia, A smart material microamplification mechanism fabricated using LIGA, Smart Mater. Struct. 7 (1) (1998) 105, https://doi.org/ 10.1088/0964-1726/7/1/012
- [35] N. Lobontiu, E. Garcia, Analytical model of displacement amplification and stiffness optimization for a class of flexure-based compliant mechanisms, Comput. Struct. 81 (32) (2003) 2797–2810, https://doi.org/10.1016/j.compstruc.2003.07.003.
- [36] L. Clark, B. Shirinzadeh, J. Pinskier, Y. Tian, D. Zhang, Topology optimisation of bridge input structures with maximal amplification for design of flexure mechanisms, Mech. Mach. Theory 122 (2018) 113–131, https://doi.org/10.1016/j.mechmachtheory.2017.12.017.
- [37] F. Chen, Z.J. Du, M. Yang, F. Gao, W. Dong, D. Zhang, Design and analysis of a three-dimensional bridge-type mechanism based on the stiffness distribution, Precis. Eng. 51 (2018) 48–58, https://doi.org/10.1016/j.precisioneng.2017.07.010.
- [38] G. Hao, J. Yu, H. Li, A brief review on nonlinear modeling methods and applications of compliant mechanisms, Front. Mech. Eng. 11 (2) (2016) 119–128, https://doi.org/10.1007/s11465-016-0387-9.
- [39] S. Awtar, S. Sen, A generalized constraint model for two-dimensional beam flexures: nonlinear strain energy formulation, J. Mech. Des. 132 (8) (2010), 081009, https://doi.org/10.1115/1.4002006.
- [40] M. Ling, J. Cao, Z. Jiang, J. Lin, Theoretical modeling of attenuated displacement amplification for multistage compliant mechanism and its application, Sens. Actuators A 249 (2016) 15–22, https://doi.org/10.1016/j.sna.2016.08.011.
- [41] Z. Yang, J. Zu, High-efficiency compressive-mode energy harvester enhanced by a multi-stage force amplification mechanism, Energy Convers. Manag. 88 (2014) 829–833, https://doi.org/10.1016/j.enconman.2014.09.026.
- [42] S. Wen, Q. Xu, Design of a novel piezoelectric energy harvester based on integrated multistage force amplification frame, IEEE/ASME Trans. Mechatron. 24 (3) (2019) 1228–1237, https://doi.org/10.1109/tmech.2019.2906999.
- [43] L.J. Lai, Z.N. Zhu, Design, modeling and testing of a novel flexure-based displacement amplification mechanism, Sens. Actuators A 266 (2017) 122–129, https://doi.org/10.1016/j.sna.2017.09.010.
- [44] W. Dong, F. Chen, F. Gao, M. Yang, L. Sun, Z. Du, J. Tang, D. Zhang, Development and analysis of a bridge-lever-type displacement amplifier based on hybrid flexure hinges, Precis. Eng. 54 (2018) 171–181, https://doi.org/10.1016/j.precisioneng.2018.04.017.
- [45] Y. Ding, L.J. Lai, Design and analysis of a displacement amplifier with high load capacity by combining bridge-type and Scott-Russell mechanisms, Rev. Sci. Instrum. 90 (6) (2019), 065102, https://doi.org/10.1063/1.5091672.
- [46] P. Schmitt, M. Hoffmann, Engineering a compliant mechanical amplifier for MEMS sensor applications, J. Microelectromech. Syst. 29 (2) (2020) 214–227, https://doi.org/10.1109/imems.2020.2965260.
- [47] M.P. Dang, H.G. Le, N. Le Chau, T.P. Dao, A multi-objective optimization design for a new linear compliant mechanism, Optim. Eng. 21 (2) (2019) 673–705, https://doi.org/10.1007/s11081-019-09469-8.
- [48] Q. Wang, J. Wei, Y. Long, J. Tan, Topology optimization design of compliant amplification mechanisms with low parasitic displacement, J. Micromech. Microeng. 33 (2) (2022), https://doi.org/10.1088/1361-6439/aca4dc.

- [49] M. Liu, X. Zhang, S. Fatikow, Design and analysis of a high-accuracy flexure hinge, Rev. Sci. Instrum. 87 (5) (2016), 055106, https://doi.org/10.1063/1.4948924.
- [50] G. Hao, X. He, S. Awtar, Design and analytical model of a compact flexure mechanism for translational motion, Mech. Mach. Theory 142 (2019), https://doi.org/10.1016/j.mechmachtheory.2019.103593.
- [51] G. Hao, J. Yu, Design, modelling and analysis of a completely-decoupled XY compliant parallel manipulator, Mech. Mach. Theory 102 (2016) 179–195, https://doi.org/10.1016/j.mechmachtheory.2016.04.006.
- [52] S. Awtar, S. Sen, A generalized constraint model for two-dimensional beam flexures: nonlinear load-displacement formulation, J. Mech. Des. 132 (8) (2010), 081008, https://doi.org/10.1115/1.4002005.
- [53] S. Awtar, A.H. Slocum, E. Sevincer, Characteristics of beam-based flexure modules, J. Mech. Des. 129 (6) (2006) 625-639, https://doi.org/10.1115/1.2717231.
- [54] J. Juuti, K. Kordás, R. Lonnakko, V.P. Moilanen, S. Leppävuori, Mechanically amplified large displacement piezoelectric actuators, Sens. Actuators A 120 (1) (2005) 225–231, https://doi.org/10.1016/j.sna.2004.11.016.
- [55] J. Zhu, G. Hao, S. Li, X. Kong, A compact mirror-symmetrical XY compliant parallel manipulator for minimizing parasitic rotations, J. Mech. Des. 144 (7) (2022), https://doi.org/10.1115/1.4053818.
- [56] G. Hao, A 2-legged XY parallel flexure motion stage with minimised parasitic rotation, Proc. Inst. Mech. Eng. Part C J. Mech. Eng. Sci. 228 (17) (2014) 3156–3169, https://doi.org/10.1177/0954406214526865.